EVALUATING SIMULATIONS AGAINST MEASURED RADAR SPECTRA FROM AN AVALANCHE EVENT

Peter Gauer*[1], Callum Tregaskis[1], Anselm Köhler[2], Anna Wirbel[2], Richard Koschuch[3]

[1] *Norwegian Geotechnical Institute, Norway*
[2] *Austrian Research Centre for Forests (BFW), Department for Natural Hazards, Innsbruck, Austria*
[3] *IBTP Koschuch e.U., Austria*

ABSTRACT: One major purpose of avalanche test sites such as Ryggfonn is to obtain measurements that can be used to characterize avalanche dynamics and to support the development, calibration, and benchmarking of numerical models. Observations often consist of point measurements or observed quantities differ from the direct result variables of numerical models which are mostly flow thickness and flow velocity in a terrain-following or cartesian coordinate system. Furthermore, simulations are subject to uncertainties in input parameters, such as release height and snow properties, for individual events. Consequently, developing robust methods for comparing observations with model results is a task in its own right.

In this paper, we present an approach for comparing radar measurements with model outputs. To this end, MTI plots and range-gate spectra derived from radar measurements are compared with corresponding synthetic MTI plots and range-gate spectra generated from model outputs. Although the two types of data are not fully comparable, the comparison reveals discrepancies between measurements and simulations and highlights shortcomings in the current modelling approaches.

KEYWORDS: avalanche dynamics; measurements; radar velocity spectra; synthetic spectra

1. INTRODUCTION

Until now, avalanche model calibration has relied predominantly on observations of avalanche runout, such as those reported by Buser and Frutiger (1980). These observations form, in a sense, the foundation for the widely used μ and ξ parameter tables for Voellmy-type models. Gauer, Body, et al. (2023) demonstrated the limitations of calibrating avalanche models using only a single constraint, namely the runout length.

Avalanche measurements are intended, among other purposes, to provide data for the development and calibration of numerical models. However, directly comparing model results with field observations is rarely straightforward. Observations often consist of point measurements, while simulations are subject to uncertainties in input parameters, such as release height and snow properties, for individual events. Thus, developing methods for systematically comparing observations with model results is a task in its own right.

Fischer (2013) proposed the Automated Indicator-based Model Evaluation and Comparison (AIMEC) approach for comparing two-dimensional modelling results. Rauter and Köhler (2019) compared the temporal evolution of the front and tail positions of measured and simulated avalanches using Moving Target Identification (MTI) plots. However, their analysis focused mainly on similarities in the temporal development of avalanche approach and length.

The spectral information contained in MTI plots may provide additional constraints for model–observation comparisons. Synthetic MTI plots generated from model outputs can provide information on the temporal evolution of the simulated avalanche, including its spatial distribution and velocity. An even more direct comparison can be made between the measured radar spectrum at a specific range gate and the corresponding synthetic radar spectrum derived from a simulation. Such comparisons may reveal discrepancies between measurements and simulations that are not apparent from runout or front and tail positions alone.

Here, we present preliminary examples of these types of comparisons using measurements from the 11 April 2021 event at Ryggfonn and simulations with parameters selected to represent the observed avalanche size and expected return period. We compare both synthetic and measured MTI plots and radar velocity spectra to assess their potential for evaluating avalanche model performance.

2. MEASURED RADAR SPECTRA

2.1. Radar Measurements

One major purpose of the Ryggfonn test site is to obtain measurements for characterizing avalanche dynamics and for benchmarking the development

* *Corresponding author address:*
Peter Gauer, Norwegian Geotechnical Institute,
P.O. Box 3930 Ullevål Stadion, NO–0806 Oslo, Norway
Tel: ++47 45 27 47 43; Fax: ++47 22 23 04 48;
E-mail: peter.gauer@ngi.no

https://doi.org/10.15788/1790098779

Figure 1: Antenna and box of the 10 GHZ Pulse-Doppler-radar (left) and view on to the avalanche track (right).

and calibration of numerical models. To this end, an autonomous Pulse-Doppler radar has been installed at the site in cooperation with the BFW in Innsbruck (Fig. 1). The radar is one of several instruments used to measure avalanche dynamics at the test site Gauer and Kristensen (cf. 2016).

A Pulse Doppler Radar emits short pulses. The pulse length in time corresponds to a range gate length in space on the slope. The intensity of the returned signal provides information on the strength of the radar backscatter, while the Doppler shift provides information on the velocity of the moving targets. Thus, for each range gate and at a given timestamp, the radar simultaneously provides information on the distribution of velocities and backscatter intensities within the avalanche. The latter may provide an indication of the concentration or size of radar-scattering particles, although its interpretation in terms of avalanche mass requires further investigation. A brief description of typical radar-derived quantities can be found in (Gauer, Kern, et al. 2007).

Several parameters relevant to avalanche dynamics can be derived from the Pulse-Doppler radar signal. For example, the arrival time of the avalanche at different range gates can be used to estimate the propagation velocity of the avalanche front. For each range gate, the radar also provides a velocity spectrum, from which characteristic or maximum particle velocities can be identified. The distribution of spectral energy over velocity may provide information on the dominant velocity of the moving avalanche mass. Furthermore, the width and shape of the velocity spectrum may contain information about the velocity variability and potentially the turbulence within the flow. A closer examination of the temporal evolution of the spectra may also provide information on the transition from the flowing to the depositional phase of the avalanche.

2.2. Event RGF 2021-04-11

The avalanche on 2021-04-11 was artificially trigger. A summary of the raw data and observations of the event can be found in (Gauer, Langeland, et al. 2022). The main release area had a size of about 1.5 ha slope parallel and a fracture depth of roughly 1 m slope normal resulting in an estimated initial mass of approx. 3×10^6 kg. In respect to runout, the calculated return period for this event is about 15–30 years. The avalanche was one of or the fastest avalanche observed at the test site. For comparison, Fig. 2 shows a summary of measurements of front velocities along the entire Ryggfonn track as well as observations between specific points at RGF.

It took the avalanche approximately 49 s to travel from the release area to the foot of the catching dam in the runout zone. This corresponds to a mean frontal velocity of approximately 38 m s^{-1}. Figure 3 shows the MTI plot and the corresponding velocity plot for this event. An MTI (Moving Target Indication) plot is a radar image showing changes in radar backscatter over time after stationary or slowly varying background reflections have been filtered out. Higher intensities correspond to stronger radar returns from features undergoing temporal changes. The backscatter intensity is influenced by both the amount of moving material and the radar cross-section of the indi-

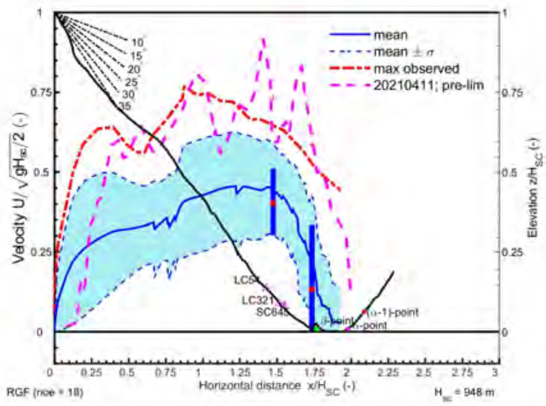

Figure 2: Range of typical front velocities along the Ryggfonn track. The blue line shows the mean, the shaded area the $\pm\sigma$-range and the red dashed-dotted line the observed maximum until 2021 derived from observations along the track. The red dashed line shows the recent event from 2021-04-11. In addition, bars show the interquartile range of the front velocity U_{LC} measured between load plates LC54 and LC321 and the front velocity U_b at the base of the catching dam, the red dots show the corresponding means and red crosses mark the measured maxima.

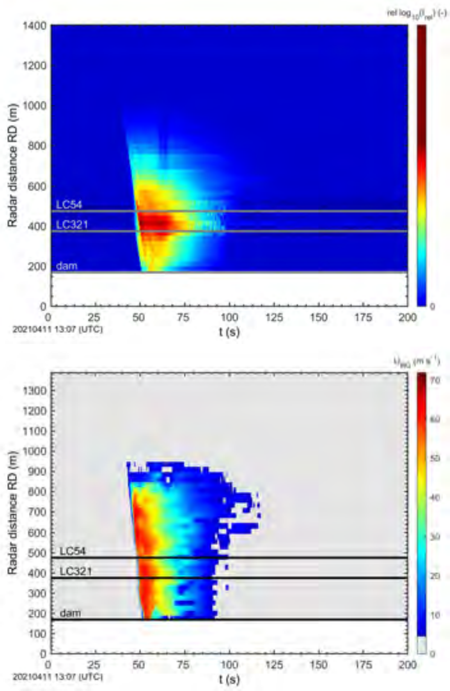

Figure 3: MTI plot (top; colors are not to scale) and corresponding velocity derived from the 0.9 quantile of the intensity response (bottom).

vidual particles. Consequently, the backscatter intensity should be regarded only as a proxy for the amount of moving mass.

As indicated by the MTI plot, the avalanche reached the dam after approximately 49 s, and the steepness of the front in the MTI plot provides an indication of the frontal velocity. The width of the signal indicates that the main body of the avalanche took approximately 30–40 s to pass a given location along the track, at least within the section covered by the radar.

The bottom panel of Figure 3 shows the corresponding Doppler velocities at the 0.9 quantile of the velocity spectra. The figure indicates that a major part of the avalanche passed through the monitored area with internal velocities of approximately 40–60 m s^{-1}. After this passage the velocities rapidly dropped. Following the passage of the main avalanche, the velocities decreased rapidly. This behavior can also be observed in the velocity spectra shown in Fig. 4, which presents the velocity spectra at three locations along the track: LC54 (RG13), LC321 (RG09), and the uphill foot of the dam (RG01). In addition, the widening of the spectra indicates that significant portions of the moving mass are decelerating and beginning to deposit. In addition, the widening spectra show that significant parts of the moving mass decelerates and begins to deposit. The entire passage of the avalanche through the respective range gate

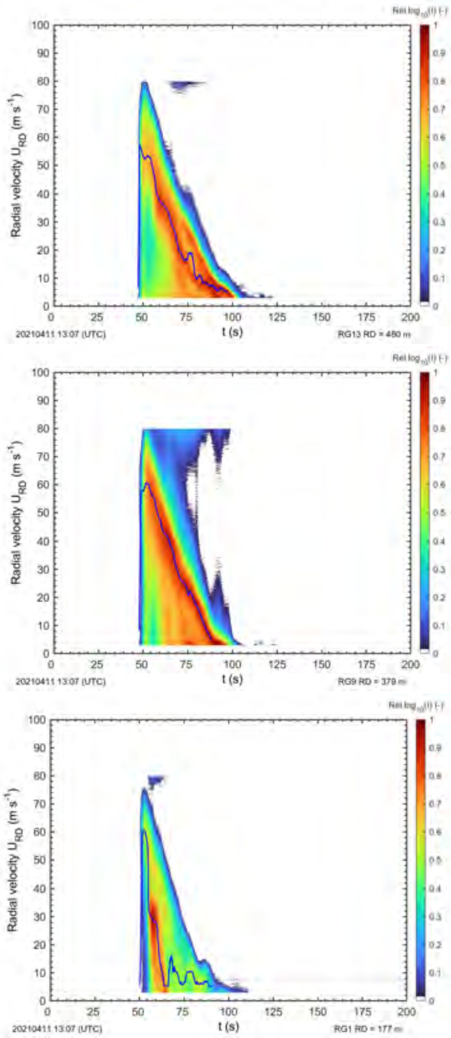

Figure 4: Velocity spectra at range gates RG13, RG09, and RG01. The blue line indicates the 0.9 quantile of the velocity spectra.

lasted approximately 50 s.

3. SYNTHETIC RADAR SPECTRA

3.1. Methodology

For comparison between the measurements and simulations, synthetic radar spectra are derived from the simulation results. To this end, velocity data are extracted at 0.05 s intervals, corresponding approximately to the sampling interval of the radar. In a second step, the velocity data for each time step are separated using a mask representing an artificial radar range gate. Figure 5 shows the typical arrangement of the range gates at the Ryggfonn site, together with a schematic illustration of the method used to extract the synthetic radar spectra. For each time step and pseudo-range gate, a histogram of the velocity distribution is calculated, analogous to the velocity spectra obtained from the radar measurements. In this way, the total number of cells within a range gate with

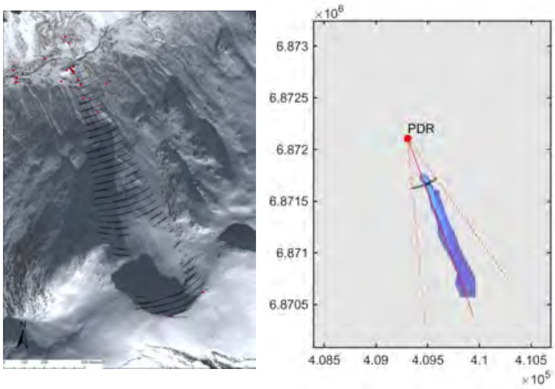

Figure 5: Radar range gates (left) and an example of the mask used to derive the synthetic radar spectra (right). The simulated velocity field at the corresponding time step is shown in the background. The red dotted lines indicate the radar opening angle and radar axis. The circular arc with a width of 25 m represents a range gate. In 2021, range gate RG01 started at a radial distance of approximately 177 m from the radar.

velocities exceeding zero or a specified threshold can be quantified and used as a proxy for radar intensity. These post-processing steps produce data that are directly comparable to the radar measurements.

3.2. MOT-Voellmy (standard)

As a first example, Fig. 6 and Fig. 7 show the MTI plot, the corresponding velocity of the "maximum intensity", and the synthetic velocity spectra for the three selected locations for one simulation. The simulation was performed with MoT-Voellmy using the standard parameter set for the size and expected return period of the event without erosion. MoT-Voellmy uses an approach similar to that of RAMMS::Avalanche (Bartelt et al. 2024) to define the parameter set.

First, it is evident from the front line in the MTI plot that the simulated avalanche took approximately 83 s to reach the foot of the dam, compared with only 49 s for the observed avalanche. This indicates that the simulation substantially underestimates the avalanche velocity in this case. This is a common phenomenon when using a Voellmy-type model with typical parameter choices. Second, although the simulation terminated according to the specified stopping criterion, movement was still ongoing after approximately 110 s, by which time most of the observed avalanche appears to have come to a stop.

The low velocity are also visible in the velocity spectra. The velocity at RG13 indicates that the main part of the avalanche flows at approximately

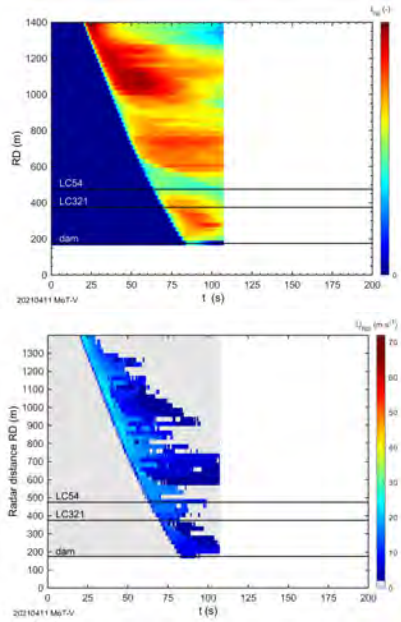

Figure 6: MTI-plot (left; colors are not to scale) and corresponding velocity of the maximum intensity (right).

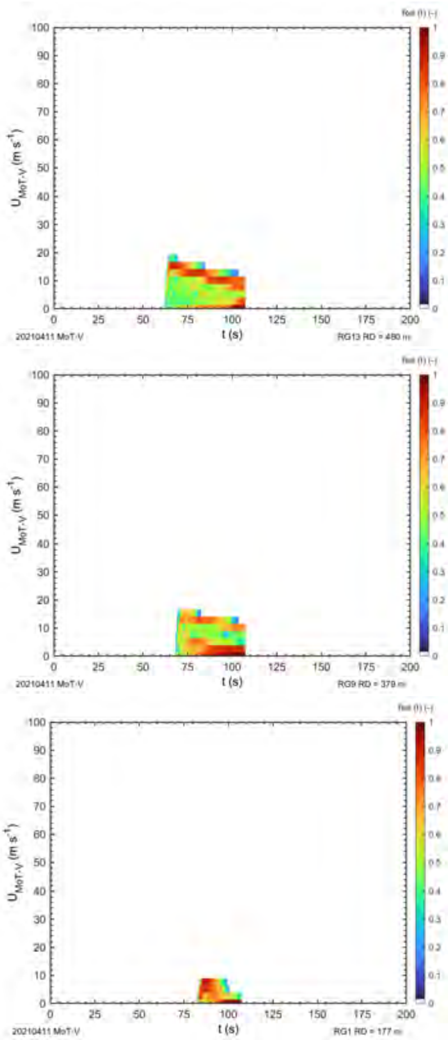

Figure 7: Velocity spectra at range gates RG13, RG09, and RG01.

10–20 m s^{-1}. Only towards the end of the simulation does a larger portion of the avalanche appear to decelerate and start depositing. At RG09, contributions at low velocities, indicative of the onset of deposition, appear much earlier and are more pronounced.

3.3. MOT-Voellmy (optimized)

In the next example, MoT-Voellmy is used again, but with optimized and fixed parameters of $\mu = 0.3$ and $k = 0.001$, again disregarding erosion. The latter parameter corresponds to approximately $\xi \approx 10^4$ m s^{-2} in RAMMS. This parameter set is close to that proposed by Gauer (2020) for a mass block model. The optimization results in the avalanche reaching the foot of the dam after approximately 50,s, as can be seen in the MTI plot in Fig. 8. In this case, the simulated velocities within the avalanche reach 40–50 m s^{-1}, which is much closer to the observed velocities. However, movement within the avalanche body still appears to persist longer than observed. The velocity spectra in Fig. 9 suggest an onset of deposition much earlier at the higher range gate. This can likely be attributed to the higher friction coefficient μ, which allows the avalanche mass to stop at higher slope angles compared with the standard parameter set. In RG13 and RG01, the onset of deposition of individual branches of the avalanche can be clearly identified.

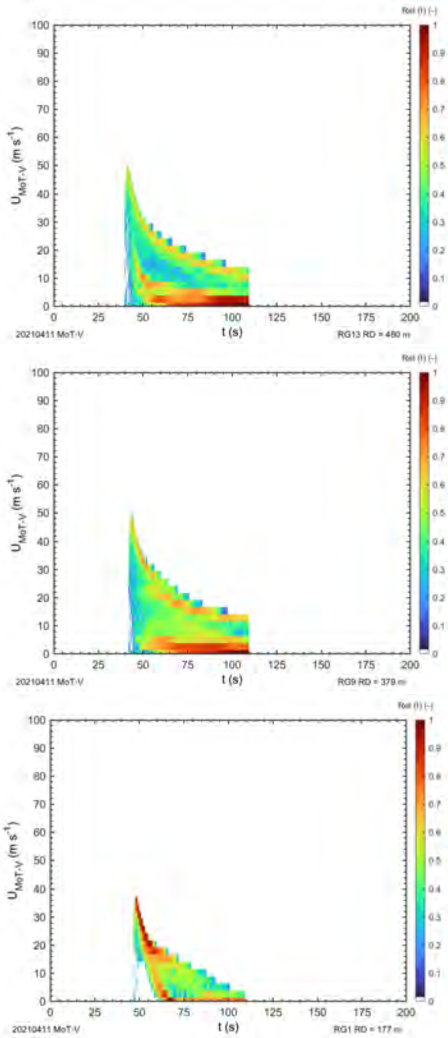

Figure 9: Velocity spectra at range gates RG13, RG09, and RG01.

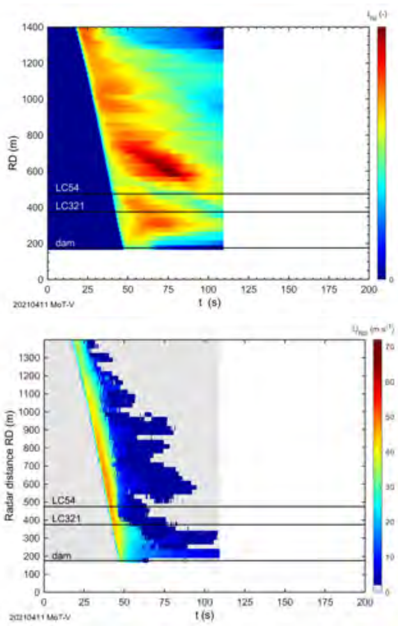

Figure 8: MTI-plot (left; colors are not to scale.) and corresponding velocity of the maximum intensity (right).

3.4. SAMOS-AT

The last example shows a simulation with SAMOS-AT, using a modified friction law that favors Coulomb-type behavior ($\mu = 0.29$, $C_D \rho_a = 0.025$ kg m^{-3}, and $\tau_c = 100$ Pa), similar to the law proposed for a mass-block model in (Gauer 2020) and to that used in (Gauer, Body, et al. 2023). In this case, possible erosion is included in the simulation. The avalanche reaches the foot of the catching dam after approximately 50 s. However, both the MTI plot and the velocity spectra suggest a more compact motion of the avalanche as a whole, resembling that of a block approximately 200–300 m in length. The velocity of the maximum intensity is again within the range of the observed values, but remains somewhat lower, as might be expected since depth-averaged models do not account for turbulent contributions. There are fewer indications of the onset of deposition than in the previous simulations.

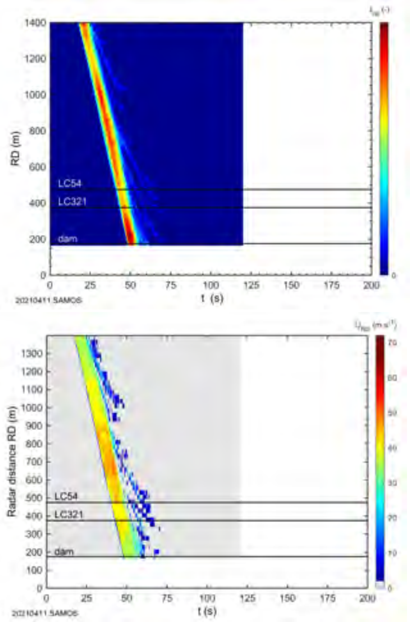

Figure 10: MTI-plot (left; colors are not to scale) and corresponding velocity of the maximum intensity (right).

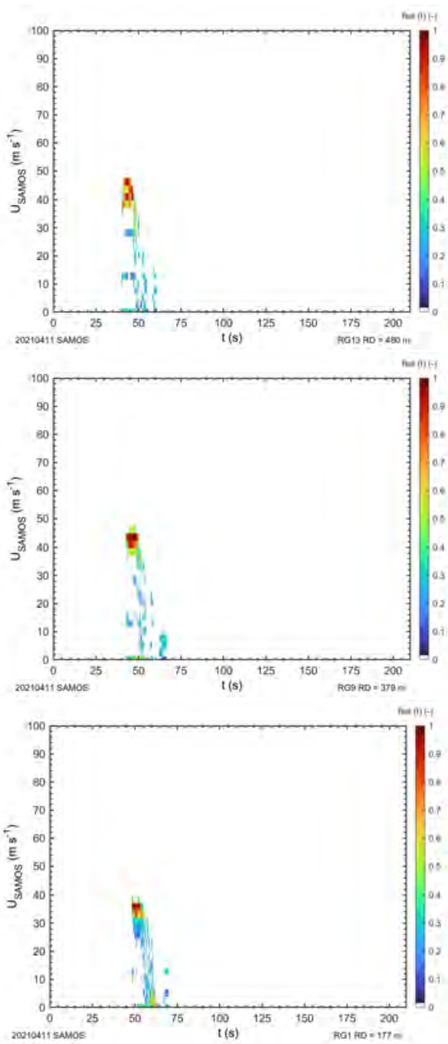

Figure 11: Velocity spectra at range gates RG13, RG09, and RG01.

4. CONCLUDING REMARKS

This paper explores the possibility of using radar measurements more directly for model verification and validation purposes. To this end, we extracted a type of synthetic radar spectrum from the simulation results and investigated the similarities and differences between the simulated and measured spectra. Although the two are not fully comparable, this approach can provide valuable insights into model behavior. As with the measured radar spectra, the synthetic spectra can be compared using various metrics, each providing different information and perspectives on model performance. The next step will be to investigate these different perspectives in more detail to gain a better understanding of their potential and limitations.

An additional advantage of using synthetic radar spectra is that the approach could potentially be extended beyond velocity measurements. For example, synthetic radar spectra could be used to investigate the development of flow depth in the model, potentially providing additional information on model performance.

ACKNOWLEDGEMENTS

Parts of this study were conducted within the NGI project Applied Avalanche Research in Norway (AARN), funded by the Norwegian Ministry of Petroleum and Energy through a grant administrated by the Research Council of Norway (RCN project no. 359890).

REFERENCES

Bartelt, P., Bühler, Y., Christen, M., Deubelbeiss, Y., Salz, M., Schneider, M., and Schumacher, L. (2024). RAMMS User Manual v.1.8.0 Avalanche. WSL Institute for Snow and Avalanche Research SLF.

Buser, O. and Frutiger, H. (1980). Observed maximum run-out distance of snow avalanches and the determination of the friction coefficients μ and ξ. In: Journal of Glaciology 26.94, pp. 121–130. https://doi.org/10.1017/S0022143000010662.

Fischer, J.-T. (2013). A novel approach to evaluate and compare computational snow avalanche simulation. In: Natural Hazards and Earth System Sciences 13.6, pp. 1655–1667. https://doi.org/10.5194/nhess-13-1655-2013.

Gauer, P., Kern, M., Kristensen, K., Lied, K., Rammer, L., and Schreiber, H. (2007). On pulsed Doppler radar measurements of avalanches and their implication to avalanche dynamics. In: Cold Regions Science and Technology 50, pp. 55–71. https://doi.org/10.1016/j.coldregions.2007.03.009.

Gauer, P. and Kristensen, K. (2016). Four decades of observations from NGI's full-scale avalanche test site Ryggfonn—Summary of experimental results. In: Cold Regions Science and Technology 125, pp. 162–176. https://doi.org/10.1016/j.coldregions.2016.02.009.

Gauer, P. (2020). Considerations on scaling behavior in avalanche flow: Implementation in a simple mass block model. In: Cold Regions Science and Technology 180, p. 103165. https://doi.org/10.1016/j.coldregions.2020.103165.

Gauer, P., Body, N. S., and Aalerud, A. H. (2023). “What Avalanche Observations Tell Us about the Performance of Numerical Models”. In: International Snow Science Workshop Proceedings 2023, Bend, Oregon, pp. 120–127.

Gauer, P., Langeland, H., Salazar, S., and Kristensen, K. (2022). WP2–Full-scale experiments at Ryggfonn: Ryggfonn avalanche observations 2020/2021. Tech. rep. 20200017-06-TN. Norwegian Geotechnical Institute.

Rauter, M. and Köhler, A. (2019). Constraints on Entrainment and Deposition Models in Avalanche Simulations from High-Resolution Radar Data. In: Geosciences 10.1, p. 9. https://doi.org/10.3390/geosciences10010009.